

# Collapse and Fragmentation in Finite Sheets

Andreas Burkert<sup>1</sup> and Lee Hartmann<sup>2</sup>

[burkert@usm.uni-muenchen.de](mailto:burkert@usm.uni-muenchen.de), [hartmann@cfa.harvard.edu](mailto:hartmann@cfa.harvard.edu)

## ABSTRACT

We present two-dimensional simulations of finite, self-gravitating gaseous sheets. Unlike the case of infinite sheets, such configurations do not constitute equilibrium states but instead are subject to global collapse unless countered by pressure forces or rotation. The initial effect of finite geometry is to promote concentrations of material at the edges of the sheet. If the sheet is not perfectly circular, gravitational focussing results in enhanced concentrations of mass. In the second-most simple geometry, that of an elliptical outer boundary, the general result is collapse to a filamentary structure with the densest concentrations of mass at the ends of the filament. We suggest that these simple calculations have interesting implications for the gravitational evolution of overall molecular cloud structure, envisioning that such clouds might originate as roughly sheetlike sections of gas accumulated as a result of large-scale flows in the local interstellar medium. We show some examples of local clouds with overall filamentary shape and denser concentrations of mass and star clusters near the ends of the overall extended structure, suggestive of our simple ellipse collapse calculations. We suggest that cluster-forming gas is often concentrated as a result of gravity acting on irregular boundaries; this mechanism can result in very rapid infall of gas which may be of importance to the formation of massive stars. This picture suggests that much of the supersonic “turbulence” observed in molecular clouds might be gravitationally-generated. Our results may provide impetus for further theoretical explorations of global gravitational effects in molecular clouds and their implications for generating the substructure needed for fragmentation into stars and clusters.

*Subject headings:* ISM: clouds, ISM: structure, stars: formation

## 1. Introduction

A central issue in star formation is the origin of the small-scale structure in molecular clouds which leads to the creation of stars. Many researchers have suggested that this substructure is

---

<sup>1</sup>University Observatory Munich, Scheinerstrasse 1, D-81679 Munich, Germany

<sup>2</sup>Harvard-Smithsonian Center for Astrophysics, 60 Garden Street, Cambridge, MA 02138

due to “turbulence”; complex, often supersonic, motions lead to density concentrations which then collapse to form stars (e.g., Larson 1992; Elmegreen 1997; Mac Low et al. 1998; Padoan & Nordlund 1999; Klessen & Burkert 2000, 2001; Ostriker, Gammie, & Stone 1999; Klessen, Heitsch, & Mac Low 2000; Bate, Bonnell, & Bromm 2002, 2003; Gammie et al. 2003; Li et al. 2004; see also review by Elmegreen 2002). However, the nature of these supersonic motions is far from clear, making it difficult to evaluate the role of turbulent fragmentation in star formation. For example, small-scale driving of turbulence is employed in many numerical simulations to form stellar mass concentrations, but this may not be consistent with large-scale structure such as extended massive filaments seen in many clouds (e.g., Schneider & Elmegreen 1979; Hartmann 2002). Another unresolved question is whether the periodic boundary conditions used in many simulations can really capture the essential physics of real clouds, in which material can either be accreted or ejected. More broadly, the recent recognition that molecular clouds have short lifetimes (Elmegreen 2000; Hartmann, Ballesteros-Paredes, & Bergin 2001 = HBB01) emphasize the likely role of initial conditions in establishing the turbulent velocity field, an area which has not been adequately explored.

A rather different approach to fragmentation was taken by Larson (1985), who pointed out that infinite self-gravitating sheets and filaments have a characteristic scale of fastest growth, typically a few times the sheet or filament scale height. In this scenario of gravitational fragmentation, gravity acts on a smooth distribution of material in a cloud of limited dimensionality (sheet or filament geometry) but infinite extent to produce fragments of finite mass. This model seems to avoid the need to put smaller (density or velocity) structure in “by hand”. Hartmann (2002) pointed out that the molecular cloud cores in Taurus are elongated in the direction of their host filaments, in the sense predicted by gravitational fragmentation. However, the static initial conditions assumed in the simplified Larson (1985) discussion are not consistent with observed supersonic velocity dispersions (e.g., Mizuno et al. 1995). In addition, as we show below, discarding the assumption of infinite sheets or filaments results in crucial modifications to Larson’s picture; finite sheets behave differently.

In this paper we extend Larson’s investigations to consider structure formation in sheets of finite sizes. We focus on a simplified investigation of initially homogeneous and isothermal sheets to isolate essential physics of the problem without introducing complications due to heating and cooling processes or turbulent driving. Even within this extremely limited set of conditions, we show that a rich variety of fragmenting structures can arise in gravitationally collapsing finite sheets, including multiple large concentrations that might lead to the formation of clusters and massive stars, with connecting and fragmenting filaments. Our investigations suggest that gravitationally-induced motions may be a significant and in many cases dominant contributor to supersonic motions in molecular clouds. We also suggest that boundary effects in general might play an important role; the assumption of periodic boundary conditions in simulations of cloud evolution might therefore neglect important aspects. The importance of boundary effects has first been pointed out by Bastien (1983) who studied the collapse of cylindrical clouds. Finally, we also speculate on a possible way of relating turbulent structure and initial mass functions.

## 2. Motivation

HBB01 argued that molecular clouds in the solar neighborhood are mostly formed as a result of large-scale flows, which pile up atomic gas until sufficient column densities are accumulated to shield the gas from the interstellar ultraviolet radiation field and allow molecules to form. The flows are presumed to be driven by stellar energy input, principally supernovae. The resulting clouds are then formed as wall sections of “bubbles” (e.g. Vazquez-Semadeni, Passot, & Pouquet 1995; Passot, Vasquez-Semadeni, & Pouquet 1995; de Avillez & Mac Low 2001; Wada & Norman 2001; HBB01, and references therein).

The simplest abstraction of this picture of cloud formation (which is also consistent with cloud formation behind a shock front, such as in a spiral density wave) is a flat uniform sheet of finite dimensions. While real clouds formed by flows obviously will not initially be perfectly flat or have uniform surface densities, it seems appropriate to make an initial exploration to isolate the effects of gravity on sheets with finite structure. To further simplify the analysis we assume isothermality and consider sheets that are either static or have simple, smooth velocity fields. Even with these restrictive assumptions, a wide variety of behavior results, which may have more general implications.

Before presenting the simulations, it is instructive to start by considering some analytic results and approximations which illustrate some basic properties. We start with the simple case of a static, isothermal, infinite, infinitely thin sheet with an initially constant surface mass density  $\Sigma_0$ . In this case the dispersion relation is (Larson 1985)

$$\Gamma^2 = 2\pi G \Sigma_0 k - c_s^2 k^2, \quad (1)$$

where  $\Gamma$  is the exponential growth rate. There is a critical wavenumber,

$$k_c = 2\pi G \Sigma_0 / c_s^2, \quad (2)$$

above which no exponential growth is possible; i.e. there is a minimum wavelength (a ‘Jeans’ length) for gravitational instability. Differentiating equation (1) with respect to  $k$ , one can find the wavenumber at which the exponential growth is fastest,

$$k_f = \pi G \Sigma_0 / c_s^2 = k_c/2. \quad (3)$$

This result suggests that the sheet will break up into fragments of preferred mass

$$M_f \sim \lambda_f^2 \Sigma = 4c_s^4 / G^2 \Sigma_0, \quad (4)$$

where  $\lambda_f = 2\pi/k_f$ . Similar results hold for a self-gravitating sheet of finite thickness, in hydrostatic equilibrium, with the critical wavenumber reduced by a factor of two. Fragmentation of an infinite filament similarly occurs on some small multiple of the thickness of the configuration (Larson 1985).

As pointed out by Larson (1985), although there is a critical wavelength for gravitational collapse in a uniform density medium (the Jeans length), it is difficult to fragment in such a situation,

for instance in a uniform density sphere, because the growth rate increases monotonically with increasing wavelength (decreasing wavenumber); large-scale collapse tends to overwhelm fragments (Tohline 1980). In contrast to the uniform sphere case, infinite sheet or filament models do exhibit a characteristic scale of growth. However, these initial equilibrium states require an infinite extent of the sheet or filament; and real clouds cannot be infinite. This leads to some important changes in the sheet/filament picture of fragmentation.

The gravitational potential at a point  $r$  from the center of an infinitely-thin, uniform surface density sheet of radius  $R$  is (Wyse & Mayall 1942)

$$\Phi = -4G\Sigma R E(r/R), \quad (5)$$

where  $\Sigma$  is the surface density and  $E$  is the second complete elliptic integral. The gravitational acceleration toward the center at  $r$  is

$$a_r = -\frac{\partial \Phi}{\partial r} = 4G\Sigma \frac{R}{r} [K(r/R) - E(r/R)], \quad (6)$$

where  $K$  is the first complete elliptic integral. The acceleration goes to infinity at  $d = R$ , which would not occur in a sheet with finite thickness; thus we restrict use of this equation to regions considerably more than a sheet thickness from the edge.

Figure 1 shows the acceleration in units of  $4G\Sigma$  as a function of  $r/R$ . The steep increase of inward acceleration as  $r \rightarrow R$  implies that the sheet, initially at rest, will immediately proceed to collapse, with material piling up most rapidly at the outer edge (limited by gas pressure gradients which we ignore here, i.e., we are assuming that the sheet contains many Jeans masses).

It is useful to estimate the timescale of global collapse for comparison with numerical results. Using the expansions of the  $K$  and  $E$  integrals (Abramowitz & Stegun 1972), equation (6) can be written as

$$a_r = \frac{1}{2} \frac{dv^2}{dr} = \pi G \Sigma \left[ \frac{r}{R} + \frac{3}{8} \left( \frac{r}{R} \right)^3 + \frac{45}{192} \left( \frac{r}{R} \right)^5 + \dots \right]. \quad (7)$$

Ignoring pressure support, a collapse timescale  $t_c$  can be estimated for a subregion of size  $\delta r$  lying in the inner region of the sheet of radius  $R$ . Integrating equation (7) using only the linear term, starting from rest, and assuming that  $\Sigma$  does not change significantly within the inner region (see §3.1), a typical infall velocity of the subregion is

$$v^2 = \frac{\pi G \Sigma}{R} (\delta r)^2, \quad (8)$$

and thus

$$t_c = \frac{\delta r}{v} = \left( \frac{R}{\pi G \Sigma} \right)^{1/2}. \quad (9)$$

Note that  $t_c$  is independent of the size of the region  $\delta r$ , a result that will be used in the following section. While this collapse timescale ignores the non-linear acceleration, and thus does not describe

the pile-up of material at the edge, we find numerically that  $t_c$  is a good estimate of the time it takes for the edge of the circular sheet to fall to the center (§3.1).

Without rotation or some other motion, the ultimate fate of this circular sheet is to collapse entirely to the center. The dashed lines in Figure 1 show linear forms for  $a_r$ ; the middle dashed line indicates the situation where an outward acceleration is comparable to the first term in the expansion of equation (7) balances the inward gravitational acceleration of the inner region. Solid-body rotation, with centripetal acceleration  $a(c)_r = -\Omega^2 r \propto r$ , where  $\Omega = \text{constant}$ , could in principle be such an example, preventing collapse in the inner sheet regions. However, the non-linear acceleration as  $r \rightarrow R$  shows that such rotation cannot stop the edge from collapsing to a ring whose dimensions are set by angular momentum. Moreover, the uniformly rotating sheet, whether in the non-equilibrium case of constant surface density, or in the equilibrium case of  $\Sigma \propto [1 - (r/R)^2]^{1/2}$  (Mestel 1963), is unstable to large-scale perturbations (Hunter 1963), and generally results in large-scale redistribution of material with a concentration of mass to the center (see, e.g., Binney & Tremaine 1987, pp 374-375). Conversely, large rotation (such as indicated by the upper dashed curve) could prevent the inner region from collapsing, but only at the expense of having the interior expand and the edge collapse to an outer ring.

The finite filament exhibits similar behavior. For a uniform cylindrical filament of radius  $h$  and length  $2l$ , the acceleration toward the center at a point on axis lying a distance  $z$  from the center is

$$a_z = -2\pi G\rho \left[ 2z - (h^2 + (l+z)^2)^{1/2} + (h^2 + (l-z)^2)^{1/2} \right], \quad (10)$$

where  $\rho$  is the density of the filament. When  $l \gg h$  and considering points away from the exact end of the filament,  $l - z \gg h$ ,

$$a_z \approx -\pi G\rho h^2 \left[ (l+z)^{-1} + (l-z)^{-1} \right]. \quad (11)$$

But  $\pi\rho h^2 = m$ , the mass per unit length of the filament. Using this relation, and expanding the quantity in brackets, we have

$$a_z \approx -Gm \left[ \frac{2z}{(l^2 - z^2)} \right]. \quad (12)$$

Figure 1 also shows the acceleration of a thin filament in units of  $G\rho$ . Note that the acceleration of an infinitely thin filament goes to infinity at its edge (equation (11)), just as in the case of the infinitely thin sheet, but this singularity disappears for finite  $h$  (equation (10)).

As in the case of the sheet, solid-body rotation of the filament (lower dashed curve) can help stabilize the collapse of the inner regions, but cannot prevent the ends of the filament from collapsing initially. Alternatively, if one wants to prevent the filament ends of collapsing, the solid body rotation would force the inner regions to expand away towards the ends of the filament, resulting in concentrations at the endpoints.

These simple considerations illustrate the universal tendency for material to pile up and concentrate at edges of finite structures due to gravity. Whether the local sheet fragmentation can

take place as envisaged by Larson (1985) depends upon whether the *global* collapse overtakes or prevents *local* collapse. This is investigated numerically in the following section.

### 3. Numerical simulations

The numerical calculations are performed on a two-dimensional Eulerian, Cartesian grid. The full computational region with dimension  $2 \times L$  is represented by a grid, composed of  $N \times N$  grid cells, equally spaced in both directions. Under the assumption of isothermality, the relevant differential equations to be integrated are the hydrodynamical continuity and momentum equations:

$$\begin{aligned} \frac{\partial \Sigma}{\partial t} + \vec{\nabla} \cdot (\Sigma \vec{v}) &= 0 \\ \frac{\partial \vec{v}}{\partial t} + (\vec{v} \cdot \vec{\nabla}) \vec{v} &= -\frac{\vec{\nabla} P}{\Sigma} - \vec{\nabla} \Phi \end{aligned} \quad (13)$$

where  $\Sigma(\vec{x})$ ,  $P(\vec{x})$  and  $\vec{v}(\vec{x})$  are the gas surface density, pressure and two-dimensional velocity vector at position  $\vec{x}$ , respectively. The gravitational potential  $\Phi$  is determined, solving Poisson's equation in the equatorial plane (Binney & Tremaine 1987)

$$\nabla^2 \Phi = 4\pi G \Sigma \quad (14)$$

with  $G$  the gravitational constant. The isothermal equation of state

$$P = c_s^2 \Sigma \quad (15)$$

determines the pressure for a given surface density  $\Sigma$  and sound speed  $c_s$ .

This set of equations is integrated numerically by means of an explicit finite second-order van Leer difference scheme including operator splitting and monotonic transport as tested and described in details in Burkert & Bodenheimer (1993,1996). In order to suppress numerical instabilities, an artificial viscosity of the type described by Colella & Woodward (1984) is added (Burkert et al. 1997).

The Poisson equation is integrated on the grid under the assumption that there is no matter outside of the computational region. As we are focussing here on the gravitationally unstable sheets that collapse towards the center of the region, outflow of gas beyond the outer boundaries can be neglected. Therefore the outflow velocities at the outer boundary are set to zero and a negligible pressure gradient is assumed. Most calculations were typically performed with  $100^2$  grid cells of size  $\Delta = 2L/N$  and height  $\Delta$ , where  $2L$  is the largest dimension of the rectangular computational

region. Test calculations with  $N=200$  and  $N=500$  did not result in significant differences. In these calculations the code units were set such that  $G = 1$ .

### 3.1. Static circular sheet

Figure 2 shows the evolution of a static sheet with initially uniform surface density (in code units,  $\Sigma = 1$ ) of circular shape, with  $R = 1$ , and sound speed  $c_s = 0.1$  (inside a computational region of  $L = 1.1$ ). The mass of this sheet is thus  $\pi\Sigma R^2 = \pi$  in code units. Larson (1985) notes that the Jeans mass for circular modes in an infinite thin static sheet is

$$M_c = 1.17c_s^4/(G^2\Sigma); \quad (16)$$

thus this sheet initially contains  $\sim 10^4$  Jeans masses. As expected, material initially piles up at the edge (left panel). Note that even at an early stage collapse in the inner regions is noticeable. The evolution of the sheet is simple; the edge grows as it falls in, and the entire structure collapses (right panel).

We never found any evidence for gravitational growth of fragments in the inner region, even for  $c_s = 0$ . Some fragmentation is seen in the piled-up ring material, which is due to growth of initial numerical noise especially on the x and y-axes, much of which is generated by the initial structure of a circular edge approximated in a rectangular grid. More and earlier fragmentation in the ring occurs as the sound speed is decreased. The details of fragmentation in this and the further simulations to be discussed should not be believed, as resolution quickly becomes an issue; here we are concentrating on global structure.

We ran a number of simulations for differing values of the sound speed; as long as the initial sheet contained many Jeans masses, i.e., the sheet was sufficiently cold, the results were similar. For warm sheets of a few Jeans masses, fragmentation due to numerical fluctuations in the edge ring was suppressed. Finally, if the mass of the sheet was small, the sheet “bounced” and then eventually adjusted to a static equilibrium.

Figure 3 shows the density and velocity structure of the simulation shown in Figure 2. Note the pile-up of material, and also that infall develops rapidly in the inner regions as well, as expected from the analytic results of the previous section. The collapse timescale in the linear (inner sheet) regime, equation (9), is  $\pi^{-1/2} = 0.564$  in code units. For the particular case described above, the time taken for the edge to reach the center is approximately  $t_g \sim 0.51$ , i.e., slightly shorter than the linear timescale.

The above result for the timescale of global vs. local collapse helps to explain why we never found any indication of small-scale, linear perturbations becoming large before the entire sheet collapsed. The infall which develops rapidly in all sheet regions apparently invalidates the linear analysis of the infinite, static sheet. Consider the following argument. The most favorable location for a finite perturbation (larger than a Jeans length) to grow before being overtaken by the general

collapse is at the center of the sheet, where the edge material takes the longest time to arrive. We may use the result of equation (9) to evaluate the timescale of local collapse in the limit of zero sound speed (negligible gas pressure) because this term simply represents gravitational acceleration. Moreover, as shown in Figure 3, even during the collapse the surface density tends to remain uniform and the velocity gradient similar until the infalling “edge” material overtakes it. Now, equation (9) indicates that the timescale for collapse is *independent* of the radius of the perturbed region; moreover, we find numerically that the time for the edge material to reach the origin is slightly less than this value. Thus, small perturbations cannot amplify before being swept up by the overall collapse. Because the collapse time (9) is proportional to  $\Sigma^{-1/2}$ , only very non-linear perturbations have a chance to grow before being swallowed up by the global collapse. The situation is analogous to the collapse of a uniform sphere, for which all radii reach the center at the same time, preventing effective fragmentation from small perturbations (Larson 1985).

Even fairly large perturbations have difficulty growing before overall collapse of the edge wins. This is shown in Figure 4, where we show the evolution of an initial 10% ring-like perturbation as a function of time. The surface density of the perturbation grows linearly with time but never outruns the edge, the latter eventually overtaking it.

### 3.2. Static ellipse

Figure 5 a-d shows the evolution of an elliptical sheet with an initial ellipticity of  $e = 0.6$ . Again, we assume  $c_s = 0.1$ . As in the case of the circular sheet, material piles up at the edge as the entire configuration collapses. However, a new feature arises: specifically, “focal points” appear, where gravity acts on the curvature of the sheet edge to produce large, dense mass concentrations close to or outside of the foci of the initial elliptical structure (upper right panel). These mass concentrations grow with respect to the rest of the edge material by gravitationally attracting neighboring material to fall into them (lower left panel). Finally, the sheet collapses into a filamentary structure with large mass concentrations at both ends.

The geometry leading to focal points is indicated schematically in Figure (6). Any sheet edge which locally has a smaller radius of curvature than the larger-scale sheet geometry will yield a local focus for gravitationally-collapsing material.

As before, our limited resolution prohibits any quantitative analysis of the number, mass, and sizes of fragments which eventually condense along the filament. The inhomogeneities present along the filament are the result of numerical noise and limited resolution (e.g., Truelove et al. 1997) which get amplified during collapse. Our main points are simply that the elongated sheet not only tends to collapse to a filament, and that focal points develop which result in larger concentrations of mass at the filament ends, a result seen, for example, in simulations of the collapse of elongated gas clouds (Bastien 1983; Bonnell et al. 1991; Burkert & Bodenheimer 1993).

### 3.3. Sheets without sharp edges

The previous calculations assumed a sharp outer edge, where the surface density decreases by two orders of magnitude. It seems implausible that real sheet-like clouds should have such sharp edges, so we investigate a case in which the transition at the cloud boundary is more gradual. Figure 7 shows what happens when the density distribution of the elliptical sheet falls off toward the edge. In this particular case the density is made to fall off smoothly to zero starting at 80% of the distance to the elliptical boundary. As shown in the left panel, an edge concentration still develops, but in a smaller structure; there is a modest amount of material outside this edge. Focal points develop as before. Finally, as shown in the right panel, collapse to a filament once again occurs, with mass concentrations near the end, but now lower-density material extends outside of the focal point concentrations. Note that Nelson & Papaloizou (1993) found that spheroids did not necessarily form concentrations at each end if the density distribution tapers off sufficiently. Uniform-density spheroids tend to have larger masses per unit lengths at their centers than the corresponding uniform sheets, suggesting that the difference between two and three dimensions can be important.

### 3.4. Expanding sheets

If sheets are made as parts of the walls of “bubbles” driven by supernova explosions or stellar winds, they will generally exhibit some expansion in the direction perpendicular to the main flow. In our two-dimensional approximation, ignoring the bubble wall curvature, we can introduce a similar effect by putting in a linear expansion term. Figure 8 shows an expanding case, which was designed such that gravity was not strong enough to reverse the expansion in the inner region, but still large enough to play a role at the outer edge. The initial radial velocity was assumed to increase linearly with distance from the center and the surface density was constant. Note that the entire region expands, but there is still a pile up of material at the edge and the formation of focal points. Thus expansion does not qualitatively change the mass concentration, though it prevents the overall collapse of the sheet.

### 3.5. Rotating sheets

In general there can be some angular momentum present in the plane of the sheet. Figure 9 shows the case of an uniformly rotating, elliptical sheet. Again focal points form and collapse to a filament eventually occurs, with larger mass concentrations at the ends of the filament (see also earlier work by Bonnell et al. 1991, Nelson & Papaloizou 1993, and Monaghan 1994.) The rotation of the resulting filament (Figure 10, left panel) is sufficient to slow the overall collapse. Material along the filament starts to be pulled in by the focal point concentrations near the ends of the filament.

We again emphasize that the number and properties of fragments in the filament is not quantitatively reliable. (Note that fragmentation of rotating filaments has also been found e.g. by Monaghan (1994).) Nevertheless, as a qualitative result it is interesting to inquire what velocity structure would be seen by an observer in the plane of the sheet (now the plane of the filament). The right panel of Figure 10 shows a contour plot of surface density integrated along the y-direction as a function of the velocity in the x-direction, when the two edges have merged into the connecting filament. In addition to the evident overall rotation, there are local velocity perturbations due to the gravitational accelerations of the various mass concentrations, (an effect earlier seen in the simulations of fragmenting cylindrical clouds by Bonnell & Bastien 1993; e.g., their Figures 3-5). The original total mass of the ellipse was 1.26 in code units, and the initial major axis was unity, so one would expect gravitationally-induced velocities to be of order  $v_{dyn} \sim (GM/R)^{1/2} \approx \text{unity}$ ; the overall velocity gradient in the line of sight is in agreement with this estimate. The “turbulence” in the line of sight, i.e., local fluctuations due to gravitational perturbations by local concentrations, is also of this order. The qualitative idea that differing mass concentrations along a filament can (and must) induce smaller-scale velocity structure (“turbulence”) is worth noting. Our results bear an interesting qualitative resemblance to the velocity gradients seen in the  $^{13}\text{CO}$  emission of the Orion A cloud (Bally et al. 1987; see §4.2).

### 3.6. Ellipse with surface density gradient

It would be surprising if sheetlike clouds in the interstellar medium were uniform in surface density. We consider the next most complicated case, that of a uniform linear surface density gradient along the major axis of the elliptical sheet. Figure (11) shows what happens in the case where the surface density varies by a factor of four from one end of the ellipse to the other, with  $\Sigma = 2$  at the right end and  $\Sigma = 0.5$  at the left. The evolution is basically the same as that of the uniform ellipse, except that the dense edge and focal point develop only at the dense end.

### 3.7. “Ghosts”

It would be surprising if real clouds had perfectly smooth boundaries of either circular or elliptical shape. As indicated schematically in Figure (6), any irregularity with a small radius of curvature will tend to produce a concentration. To explore the qualitative nature of a complex boundary, in Figure 12 we show the results of the collapse of a sheet with uniform initial surface density but an arbitrary irregular boundary (the “ghost”). As shown in the sequence of figures, pile up of material occurs first along the edge, as before; focal points develop soon after. As collapse proceeds, more material is pulled into the focal concentrations, which fall in toward the origin. Near the end of the calculation, most of the mass lies in concentrations, in number initially reflecting the number of initial “nodes” in the original boundary; merging and subsequent evolution probably occurs but we cannot follow it in detail with our resolution.

## 4. Discussion

### 4.1. Initial conditions

Our results show the powerful tendency of finite self-gravitating sheets to develop structure as a result of gravitational focussing. This immediately raises the question: how relevant are these highly simplified calculations? Real clouds are likely to have much more initial structure than what we have imposed in our simulations; however, this should simply generate more substructure due to local focussing effects. Similarly, the overall tendency for a non-circular sheet to collapse to a filament should also be robust; more initial substructure will not stop the global collapse to a filament, though the detailed structure could be much more complex.

Because a finite self-gravitating sheet will immediately start to collapse at its edges, our assumption of static initial edge structure is probably not very realistic. However, we think that this complication does not matter very much. As real molecular clouds are accumulated out of material in the diffuse interstellar medium, collapse will start, leading to concentrations at edges some time before the final cloud mass has been accreted; but because this process is so rapid, it is not important whether or not this is regarded as an initial condition or as an early development. Perhaps our results for the sheet with a decline in density near the outer edge (Figure 11) can be thought of as indicating the evolution in a case where material is still being accumulated in outer regions as the interior collapses. As discussed in the previous sections, such edge effects can only be avoided by using substantial differential rotation or internal pressure gradients in ways that are not clearly relevant to most molecular clouds.

Of course, the formation of real clouds by flows will introduce some density inhomogeneities and velocity perturbations. Thus one can expect the structure of real clouds to develop in a much more complex way than considered here. But we suggest, as demonstrated in the following subsection, that our results may be relevant to the large-scale or overall morphology of at least some molecular clouds, with significant substructure superimposed by velocity and density perturbations.

Broadly speaking, our results are a simple case of the more general proposition of Ballesteros-Paredes, Vazquez-Semadeni, & Scalo (1999) that molecular clouds cannot be in virial equilibrium. As a technical matter, our calculations also suggest that the occasional practice in numerical simulations of “turning on” gravity after some evolution is not appropriate; gravity has long-range effects which must be considered. In addition, it seems clear that computational boxes with periodic boundary conditions will not capture potentially important evolution.

### 4.2. Cloud morphologies

It is obvious that a huge variety of shapes and fragments can result from sufficiently complicated initial conditions at sheet edges, or from a spectrum of density fluctuations within sheets. Taking the larger view, it is interesting to note that already the second-simplest figure - an elliptical sheet -

produces filaments with larger mass concentrations at each end. This result suggests that as clouds initially are likely to be non-circular even if sheetlike configurations of this type might be fairly common. Here we briefly consider the morphology of some well-known local star-forming regions in light of our simplified collapse calculations.

Figure 13 shows the large-scale distribution of  $^{12}\text{CO}$  emission in the Orion A and B clouds (Wilson 2001). The overall morphology of the clouds suggests part of an arc, such as might be produced by an expanding, flow-driven bubble which accumulates material far out of the galactic plane (HBB01). The overall structure is highly filamentary, especially in the A cloud. Strikingly, the massive Orion Nebula Cluster (Hillenbrand 1997, and references therein) and the young, dense embedded clusters NGC 2024, 2068, and 2071 (Lada 1992) lie preferentially at the ends of the molecular gas distribution, just as would be predicted by the simplest version of sheet collapse in a non-circular sheet. There are multiple condensations of molecular gas and young stars in these clouds, not just one major cluster at each end of each cloud, but such independent condensations would occur as long as the initial cloud were not a perfectly smooth ellipse in shape.

Dense clusters and dense filamentary gas lie only at one end of the Orion A cloud (e.g., Ali & Depoy 1995; Goldsmith, Bergin, & Lis 1997). The other (southern; higher galactic longitude  $l$ ) end of the cloud appears to be much more diffuse and contains only small groups of stars (e.g., Strom, Margulis, & Strom 1989; Strom, Strom, & Merrill 1993). We speculate that this difference is due to initial conditions; the cloud prior to collapse was initially much more diffuse at one end than the other. The overall structure of the A cloud suggests a “V” shape, with the dense narrowest region at the northern end (the region of the so-called “integral-shaped” filament; see Bally et al. 1987). Now, prior to overall collapse to a filament, our calculations for initially elliptical sheets show similar structure at each end; denser concentrations are formed at the “tip” of the ellipse, with two “filaments” streaming out on either side. We speculate that we are seeing a similar effect in the A cloud; the southernmost parts have not collapsed as far as the northern (lower  $-l$ ) region.

Figure 14 shows an extinction map of the Ophiuchus region, which more or less indicates the large-scale morphology of the molecular gas. The well-known filamentary structure extending outward from the main concentration of gas and dust is evident. Again, we speculate that the overall structure of this region is due to a collapse similar to that shown at either end of our elliptical sheet calculations, with a “V” of filaments extending out from the main dense collapse region. The structure is more complex than that of our elliptical sheet simulations, but then the initial conditions are unlikely to be as smooth and simple for real clouds.

Figure 15 shows the distribution of young stars and extinction (which, again, traces the molecular gas fairly well) in the Cha I cloud. Note how the cloud is filamentary, and that once again there are two clear concentrations of stars nearer the ends of the cloud.

Not all molecular clouds exhibit a simple global filament structure with clusters at the ends. Figure 16 shows the positions of the young stars in the Taurus molecular cloud, superimposed on the  $^{13}\text{CO}$  integrated emission (Mizuno et al. 1995). As noted before (e.g., Hartmann 2002, and

references therein), Taurus is composed of extended, roughly parallel bands or filaments of both gas and stars; gravitational fragmentation into several filaments may have occurred (Miyama et al. 1987a,b; Nakajima & Hanawa 1996). There are no major clusters of stars in Taurus (although there is a small double group of stars in L1495; see Figure (16)). Taurus is one of the most dispersed, extended, and low-density clouds, much more extended than regions comparable in mass such as Ophiuchus. We suggest that the small-scale density and velocity fluctuations inevitably present in any realistic scenario of cloud formation play a much larger role in Taurus than in other regions; the low surface density suggests that global gravitational collapse may not dominate the structure imposed by initial inhomogeneities, in contrast with higher surface density regions.

However, even in this case of Taurus there is some suggestive substructure. For instance, the double group of L1495 seems to lie at the end of a filament and V-shaped structure running from  $l \sim 166$  to about  $l \sim 169$ ; this gas structure seems distinct from other regions, especially as the radial velocities of the gas increase (to positive values) with increasing  $l$ , whereas the overall trend in Taurus is increasing radial velocities with decreasing  $l$  (e.g., Mizuno et al. 1995). Similarly, there is structure near  $l \sim 174$ ,  $b \sim -13.5$  (Heiles Cloud 2) which exhibits a curious oval shape with an interior hole as seen in integrated intensity; the young stars also lie along the edge of the oval, suggesting fragmentation in a collapsing cloud edge.

It is worth noting that a number of molecular clouds show a rotation or shear in the line of sight that is comparable to the gravitational acceleration, such as the Orion complex (Bally et al. 1987) and Taurus (e.g., Mizuno et al. 1997). As shown in the simulation of Figure 9 such rotation can slow or prevent the overall collapse of the filament before fragmenting and presumably forming stars. A plausible scenario would be to assume sheets with some angular momentum, insufficient to prevent collapse to a filament, but large enough that the resulting filament does not collapse completely. In this kind of picture, there would be a tendency to form filaments with significant rotational support; they would tend to shrink down until arriving at the angular momentum “barrier”.

In summary, we find that several local cloud complexes have morphologies suggestive of the simplest versions of global collapse from a sheetlike configuration; i.e., roughly filamentary cloud structure with concentrations of mass at the end(s) of the clouds.

### 4.3. Cluster formation

The simple simulations discussed here may also have particularly important implications for the formation and evolution of star clusters. Many treatments of young clusters assume something like an initial equilibrium configuration and follow the subsequent evolution. However, the simulations presented here suggest that the accumulation of protocluster gas is often a result of gravitational focussing; in other words, that the gas forming the stars is initially collapsing. Formation in collapsing media might result in violent relaxation determining the cluster structure rather than two-body interactions, a result suggested for the very young Orion Nebula Cluster by Hillen-

brand & Hartmann (1998). Violent relaxation is not restricted to initially highly gravitationally unstable conditions, like a collapsing sheet. In the absence of periodic boundary conditions, initially stabilized but efficiently dissipating turbulent clouds will evolve into global gravitational collapse while fragmenting with violent relaxation also playing some role in the late phases of evolution (Bate, Bonnell & Bromm 2003; Bonnell, Bate & Vine 2003).

Additionally, the picture presented here of cluster formation is consistent with the ideas of competitive accretion forming massive stars at the bottoms of cluster gravitational potential wells (Zinnecker 1982; Bonnell et. al. 2001a,b). It is worth noting that global infall into focal points can result in very high local mass infall rates, such as are needed to form very massive stars in short times. Alternative pictures in which high infall rates are achieved in static clouds of order one Jeans mass by invoking a high turbulent velocity to support the required high densities seem implausible. In our picture, global collapse could constitute a substantial fraction of the observed “turbulence” in dense cores, with perhaps smaller-scale structure generated by attraction to local mass concentrations.

#### 4.4. Kinematics

A further implication of the simulations is that the “turbulent” motions of many star-forming structures are not necessarily those of a Kolmogorov spectrum, but those of gravitationally-induced flows with substantially more power on large scales. Another way of saying this is that a substantial component of the observed supersonic line widths in star-forming regions could be the result of collapse rather than small-scale, random turbulent motions. Our simulations are not ideal for exploring this possibility; by restricting the motion to two dimensions and limiting the spatial resolution, we are unable to follow details of the motion. Nevertheless, the idea of global collapse as an important generator of supersonic “turbulence” is very attractive, in that some mechanism must be invoked to make gas concentrations in the first place, and star formation must involve gravitationally-bound entities.

It is worth noting that, while our non-rotating and non-expanding simulations result ultimately in collapse of all the material to the origin, many real clouds exhibit large scale velocity gradients along their lengths (e.g., Bally et al. 1987), of a magnitude comparable to that required to prevent total collapse. Such velocity gradients must be the result of initial conditions which generally provide molecular clouds with significant angular momenta.

#### 4.5. Implications for the initial mass function

Our results suggest that there might be some relation between the boundary structure of molecular clouds and the mass distributions of gravitationally-focussed concentrations, i.e. between cloud edges and stellar/cluster mass functions. Larson (1992) suggested that fractal structure in

clouds might be related to the stellar initial mass function; he speculated that the observational indication of fractal projected cloud boundaries (e.g., Falgarone et al. 1991) with fractal dimension  $D \sim 1.35$  could be translated into a mass function  $dN/d\log M \propto M^{-x}$ , with  $x \sim 2.35$ , consistent with the upper end of the stellar mass function (see also Elmegreen 1997). Our simulations suggest a physical mechanism – gravitational focussing – which can act *directly* on cloud boundaries to form mass concentrations, with a distribution that reflects the size distribution of irregularities at cloud boundaries. This idea needs further exploration, as subsequent fragmentation and/or competitive accretion could easily modify the mass function resulting simply from edge collapse.

## 5. Conclusions

Using numerical simulations of simple, isothermal, finite sheets, we have shown that gravity acting on sheet edges can produce a wide variety of structures which are likely to have some relevance to observed star-forming structures in molecular clouds. In particular, we have shown that a likely general result of the collapse of a sheet formed by flows in the ISM is a filament with higher mass concentrations at the ends of the filament. Any departure from circular symmetry at the edge of gravitationally-bound clouds will tend to produce denser concentrations that may be the origin of star clusters. Already in 1983 Bastien found that elongated cylindrical clouds fragmented into two condensations which he identified as an 'end effect' which results from a similar physical behaviour as collapsing finite sheets. We have shown that several nearby clouds exhibit morphologies which are broadly consistent with the simulations.

We have addressed the problem of finite self-gravitating sheets in as simple a form as possible, limiting the motion to two dimensions. Even with these restrictions, our results emphasize the long-range effects of gravity, and the importance of cloud boundaries, in generating structure and turbulence. It is likely that clouds are formed with much more structure than assumed here; further steps needed include simulating the formation of molecular clouds from the diffuse interstellar medium, to explore what initial density and velocity fluctuations are present. The dynamic nature of even the simple simulations presented here makes it likely that quasi-equilibrium treatments of molecular cloud structure and star formation are unlikely to be realistic. Our initial explorations emphasize the importance of gravitational focussing in creating structure and turbulence in (finite) molecular clouds, a viewpoint that may lead to new observational and theoretical approaches to understanding star formation.

Thanks to John Carpenter for providing a modified version of the Cha I cloud results and to Alyssa Goodman for the extinction map of Ophiuchus. This work was supported in part by NASA grant NAG5-9670 and NAG5-13210.

## REFERENCES

Abramowitz, M., & Stegun, I.A. 1972, Handbook of Mathematical Functions (Dover: New York), 591

Ali, B. & Depoy, D. L. 1995, AJ, 109, 709

Ballesteros-Paredes, J., Vázquez-Semadeni, E., & Scalo, J. 1999, ApJ, 515, 286

Bally, J., Stark, A. A., Wilson, R. W., & Langer, W. D. 1987, ApJ, 312, L45

Bastien, P. 1983, å, 119, 109

Bate, M. R., Bonnell, I. A., & Bromm, V. 2002, MNRAS, 332, L65

Bate, M. R., Bonnell, I. A., & Bromm, V. 2003, MNRAS, 339, 577

Binney, J. & Tremaine, S. 1987, "Galactic Dynamics" (Princeton Univ. Press)

Bonnell, I. A., Martel, H., Bastien, P., Arcorgi, J.-P. & Benz, W. 1991, ApJ, 377, 553

Bonnell, I. A. & Bastien, P. 1993, ApJ, 406, 614

Bonnell, I. A., Bate, M. R., Clarke, C. J. & Pringle, J. E. 2001a, MNRAS, 323, 785

Bonnell, I. A., Clarke, C. J., Bate, M. R., & Pringle, J. E. 2001b, MNRAS, 324, 573

Bonnell, I. A., Bate, M. R., & Vine, S. G. 2003, MNRAS, 343, 413

Burkert, A., Bate, M.R. & Bodenheimer, P. 1997, MNRAS, 289, 497

Burkert, A. & Bodenheimer, P. 1993, MNRAS, 264, 798

Burkert, A. & Bodenheimer, P. 1996, MNRAS, 280, 1190

Carpenter, J. M., Hillenbrand, L. A., Skrutskie, M. F., & Meyer, M. R. 2002, AJ, 124, 1001

Collela, P. & Woodward, P. 1984, J. Comput. Phys. 54, 174

de Avillez, M. A. & Mac Low, M. 2001, ApJ, 551, L57

Elmegreen, B. G. 2002, ApJ, 577, 206

Elmegreen, B. G. 1997, ApJ, 486, 944

Elmegreen, B.G. 2000, ApJ, 530, 277

Falgarone, E., Phillips, T. G., & Walker, C. K. 1991, ApJ, 378, 186

Gammie, C. F., Lin, Y., Stone, J. M., & Ostriker, E. C. 2003, ApJ, 592, 203

Goldsmith, P. F., Bergin, E. A., & Lis, D. C. 1997, ApJ, 491, 615

Goodman, A. 2004, ASP Conference Series, to appear (D. Johnstone & E. Ostriker, eds.)

Hartmann, L. 2002, ApJ, 578, 914

Hartmann, L., Ballesteros-Paredes, J., & Bergin, E. A. 2001, ApJ, 562, 852

Hillenbrand, L. A. 1997, AJ, 113, 1733

Hillenbrand, L. A. & Hartmann, L. W. 1998, ApJ, 492, 540

Hunter, C. 1963, MNRAS, 126, 299

Klessen, R. S. & Burkert, A. 2000, ApJS, 128, 287

Klessen, R. S. & Burkert, A. 2001, ApJ, 549, 386

Klessen, R. S., Heitsch, F., & Mac Low, M. 2000, ApJ, 535, 887

Lada, E. A. 1992, ApJ, 393, L25

Larson, R. B. 1985, MNRAS, 214, 379

Larson, R. B. 1992, MNRAS, 256, 641

Larson, R. B. 1995, MNRAS, 272, 213

Li, P. S., Norman, M. L., Mac Low, M., & Heitsch, F. 2004, ApJ, 605, 800

Mac Low, M.-M., Klessen, R. S., Burkert, A., & Smith, M. D. 1998, Phys. Rev. Lett., 80, 275

Mestel, L. 1963, MNRAS, 126, 553

Miyama, S.M., Narita, S., & Hayashi, C. 1987a, Prog. Theoretical Physics, 78, 1051

Miyama, S.M., Narita, S., & Hayashi, C. 1987b, Prog. Theoretical Physics, 78, 1273

Mizuno, A., Onishi, T., Yonekura, Y., Nagahama, T., Ogawa, H., & Fukui, Y. 1995, ApJ, 445, L161

Monaghan, J. J. 1994, ApJ, 420, 692

Nakajima, Y. & Hanawa, T. 1996, ApJ, 467, 321

Nelson, R.P. & Papaloizou, C.B. 1993, MNRAS, 265, 905

Ostriker, E. C., Gammie, C. F., & Stone, J. M. 1999, ApJ, 513, 259

Padoan, P. & Nordlund, Åke 1999, ApJ, 526, 279

Passot, T., Vazquez-Semadeni, E., & Pouquet, A. 1995, ApJ, 455, 536

Schneider, S. & Elmegreen, B. G. 1979, ApJS, 41, 87

Strom, K.M., Margulis, M., & Strom, S.E. 1989, ApJ, 346, L33

Strom, K.M., Strom, S.E., & Merrill, K.M. 1993, ApJ, 412, 233

Tohline, J.E. 1980, ApJ, 239, 417

Truelove, J. K., Klein, R. I., McKee, C. F., Holliman, J. H., Howell, L. H., & Greenough, J. A. 1997, ApJ, 489, L179

Vazquez-Semadeni, E., Passot, T., & Pouquet, A. 1995, ApJ, 441, 702

Wada, K. & Norman, C. A. 2001, ApJ, 547, 172

Wilson, A. 2001, unpublished Ph.D. thesis

Wyse, A. B. & Mayall, N. U. 1942, ApJ, 95, 24

Zinnecker, H. 1982, in *Symposium on the Orion Nebula to Honour Henry Draper*, eds. Glassfold A.E. et al. (New York: Academy of Sciences), p. 226

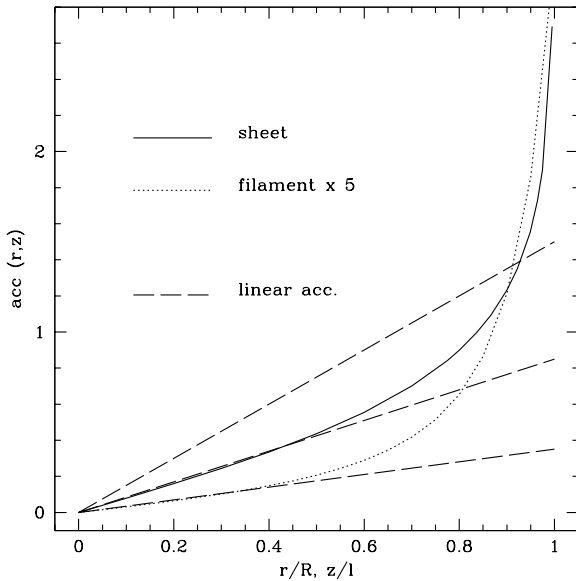


Fig. 1.— Gravitational acceleration for the uniform sheet (equation 6; solid line), in units of  $4G\Sigma$ , vs. radial distance in units of total sheet radius  $r/R$ , along with the acceleration for the uniform filament (equation 10; dotted line), in units of  $G\rho/5$ . Various linear terms are indicated by dashed lines (see text).

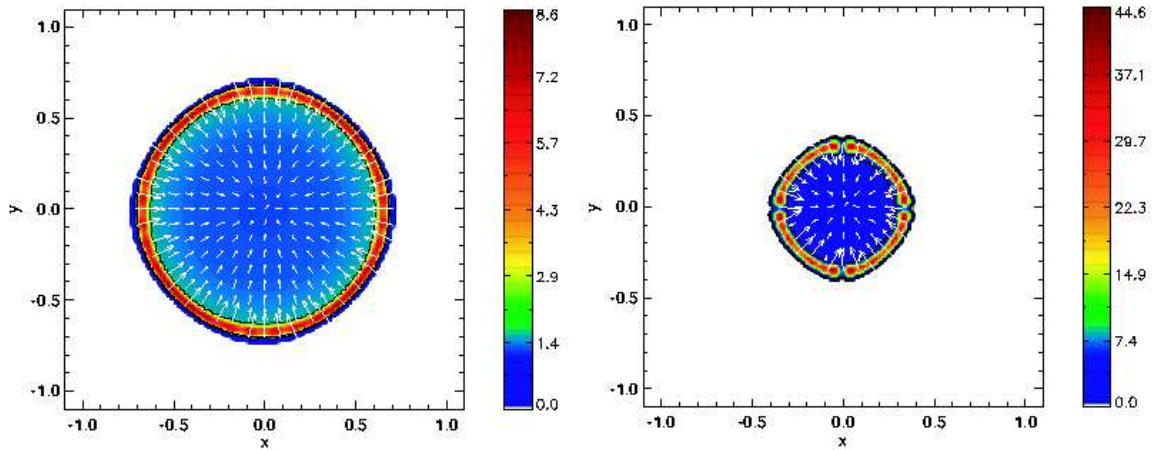


Fig. 2.— Numerical simulation of the collapse of the finite two-dimensional sheet. In this calculation the initial sheet surface density is set to unity,  $G = 1$ , and the sound speed is 0.1 in appropriate units (see text). In code units, the time at which the snapshot is taken in the left panel is 0.285; for the right panel,  $t = 0.429$ . The gaps in the outer ring on the x and y axis in the left panel are purely numerical and caused by the representation of the circular sheet by a cartesian grid.

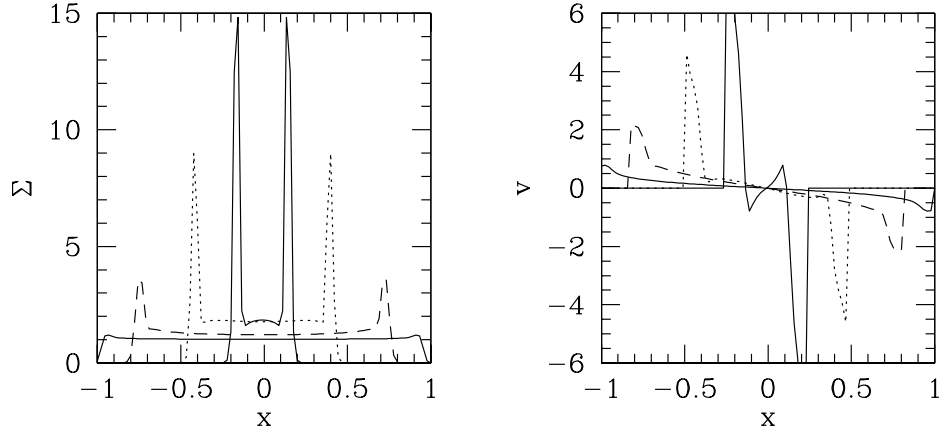


Fig. 3.— Evolution of the density and velocity of the circular sheet collapse of Figure 2. The snapshots are taken at times  $t = 0.09, 0.25, 0.41$ , and  $0.49$ . Note the flat density distribution and the linear velocity gradient in the inner regions, as expected from the result in equation (8), until late in the evolution, when inner material begins to fall outward due to the gravity of the infalling edge.

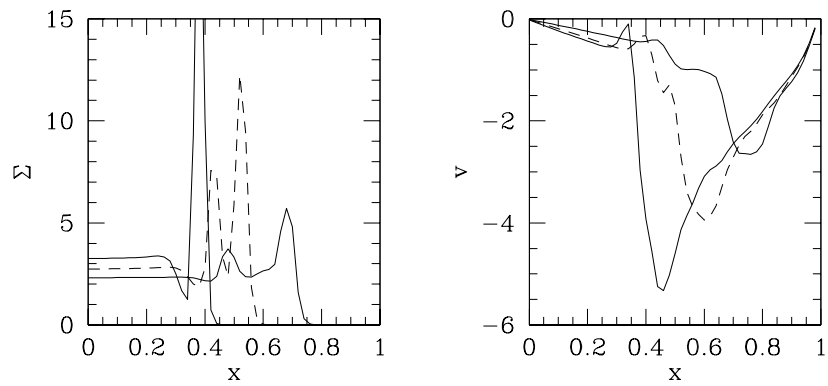


Fig. 4.— Evolution of the uniform circular sheet with a ring-like perturbation of excess surface density at times  $t = 0.15, 0.21$  and  $0.26$ . The perturbation grows as the sheet collapses, but not non-linearly, and is eventually overtaken by the collapse of the edge (see text)

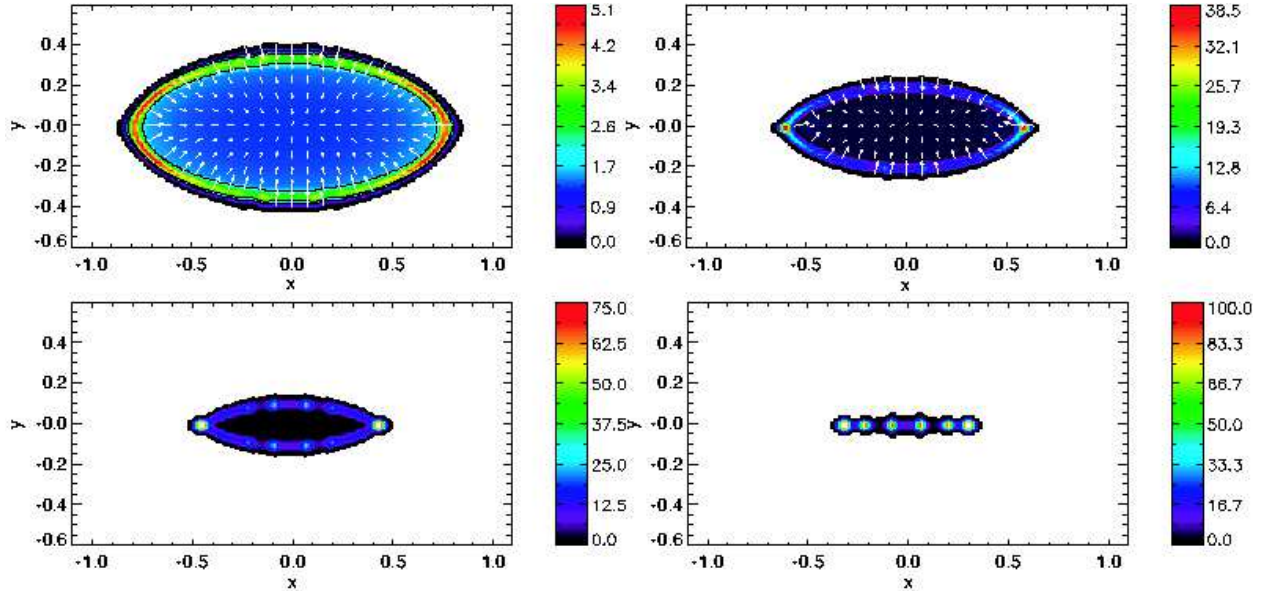


Fig. 5.— Collapse of a static elliptical sheet. Upper left:  $t = 0.23$ , material piles up at the edge as the sheet collapses. Upper right:  $t = 0.33$ , material accumulates particularly at focal points at the ends of the ellipse. Lower left:  $t = 0.39$ , focal points become more prominent. Lower right:  $t = 0.44$ , collapse to a filament has occurred, with major concentrations at the ends.

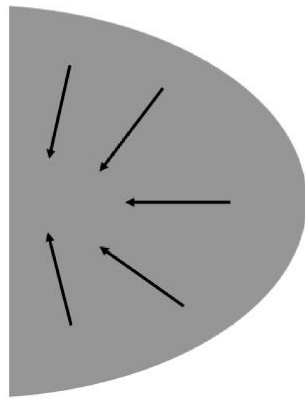


Fig. 6.— Schematic geometry leading to mass concentration at a “focal point” (see text)

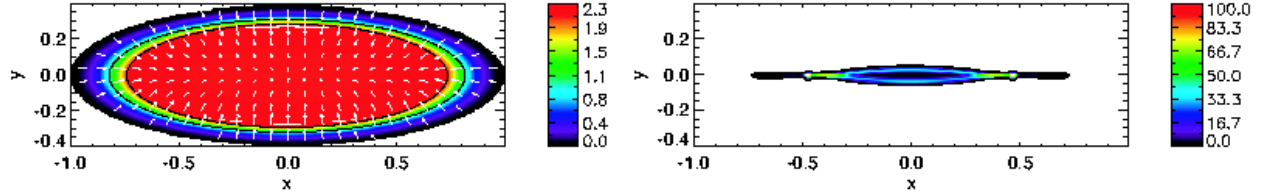


Fig. 7.— Evolution of the static elliptical sheet with density decreasing to the edge, The main features of the uniform ellipse are retained; a pile-up of material still occurs, though on a smaller scale, more material lags outside the edge (left panel), and the final filament formed shows mass concentrations somewhat interior to the ends of the filamentary gas (right panel) (see text)

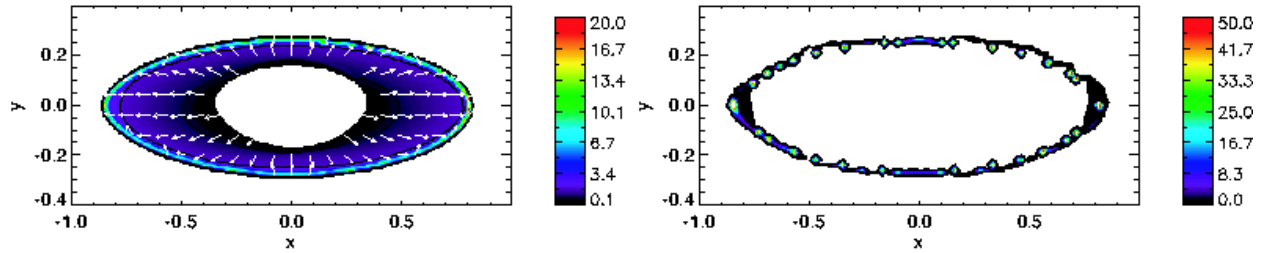


Fig. 8.— Results for an expanding elliptical sheet. Material moves outwards from the origin to add to the edge, which still forms a concentration (left panel); ultimately, most of the mass ends up in the expanding edge, with fragments determined by numerical noise and resolution (right panel) (see text)

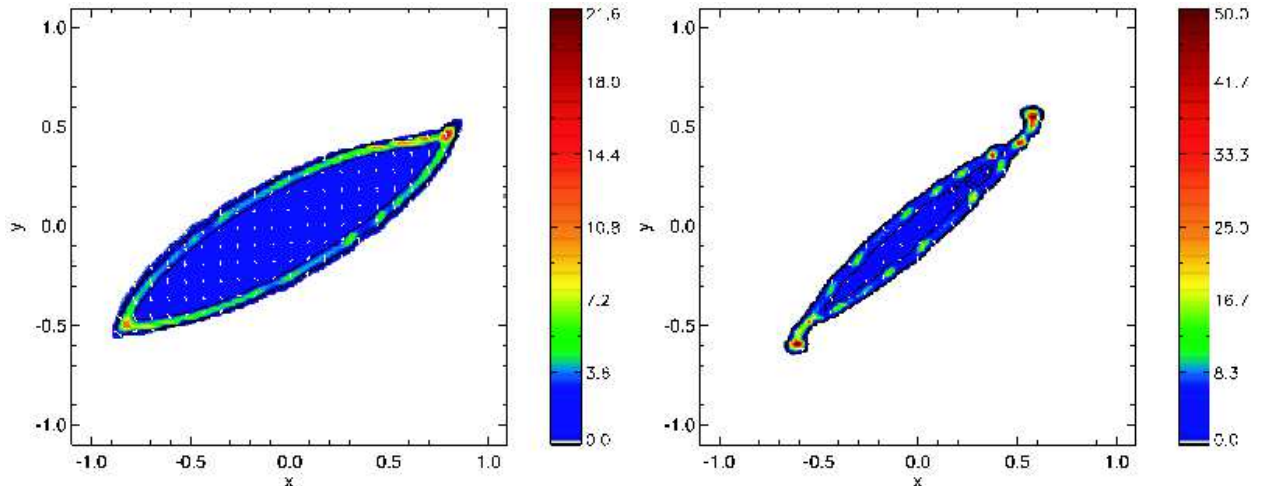


Fig. 9.— Collapse of the rigidly rotating elliptical uniform sheet. Focal points form and an eventual filament results (see also following figure) which has significant rotational support against gravity (see text)

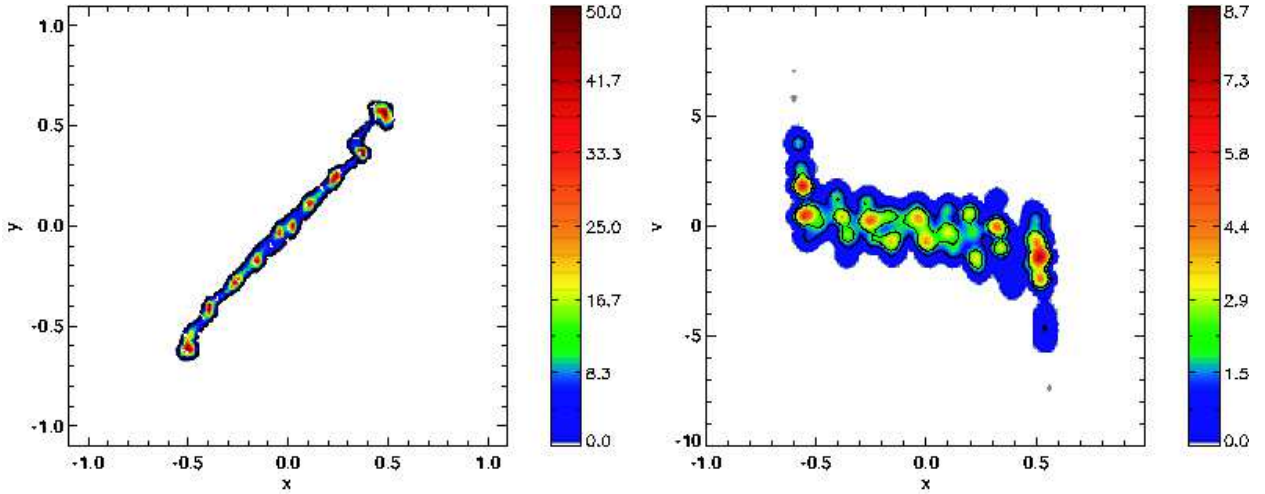


Fig. 10.— Left panel: formation of a filament from the rotating ellipse simulation (Figure 9). The size and number of subfragments are not quantitatively reliable. Right panel: contours of constant surface density integrated in the y-direction as a function of velocity in the x-direction (see text)

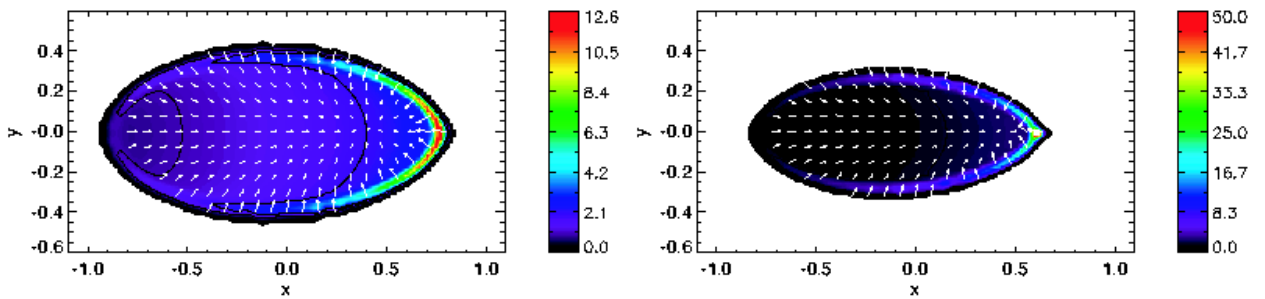


Fig. 11.— Evolution of the static elliptical sheet with a linear surface density gradient along the major axis. The resulting evolution is similar to the uniform ellipse, except that the dense edge and focal point concentration develop only at one end (see text)

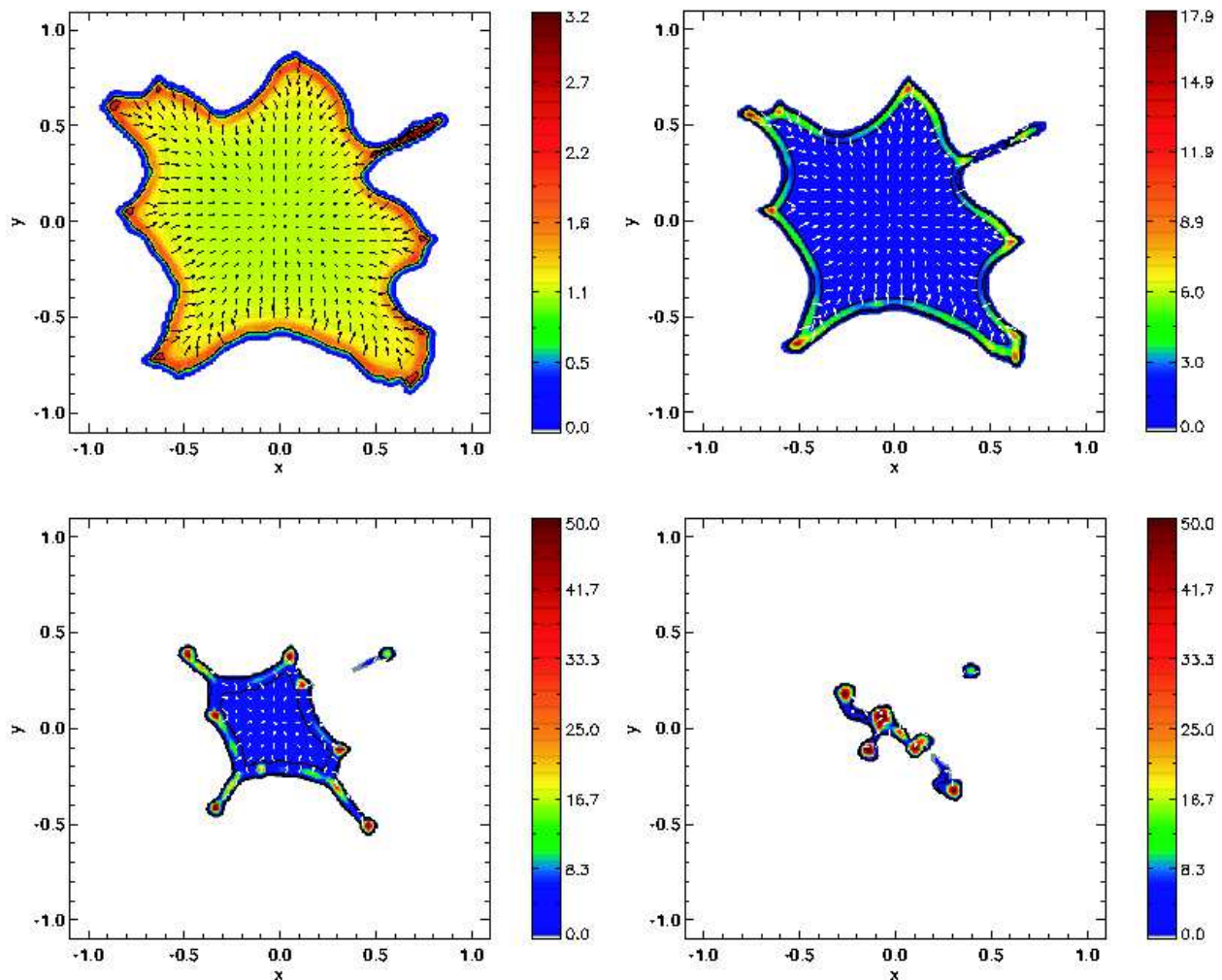


Fig. 12.— Collapse of the “ghost”, a sheet with highly irregular boundary (see text)

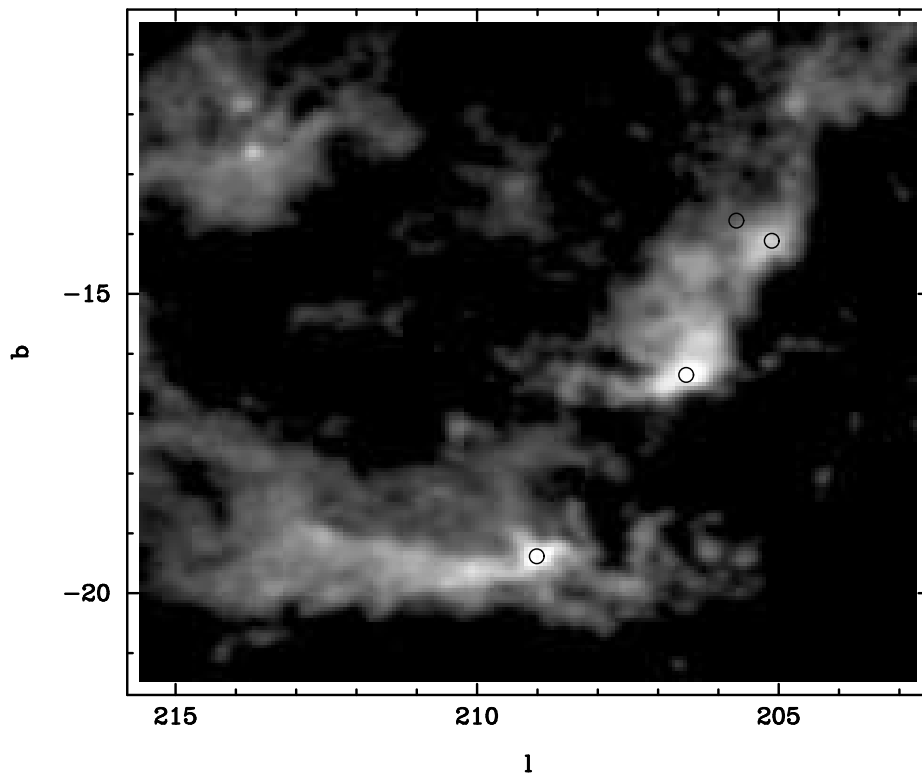


Fig. 13.— Large-scale distribution of integrated  $^{12}\text{CO}$  emission in the region of Orion, shown as a function of galactic longitude and latitude. Positions of the Orion Nebula cluster and the young NGC 2024, 2068, and 2071 clusters are marked by superimposed circles (see text). From Wilson (2001).

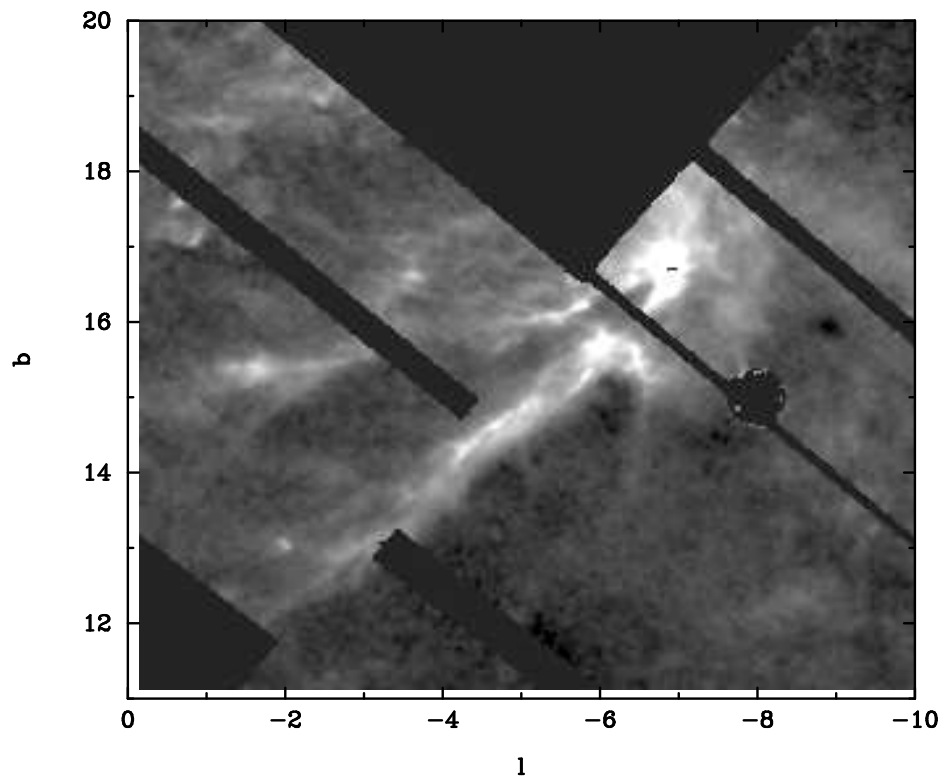


Fig. 14.— Extinction map of the Ophiuchus region, made by the COMPLETE project using 2MASS data (Goodman 2004: see also <http://cfa-www.harvard.edu/COMPLETE>). The major filamentary structures of the cloud and the main concentration of dust (and gas) are evident (see text)

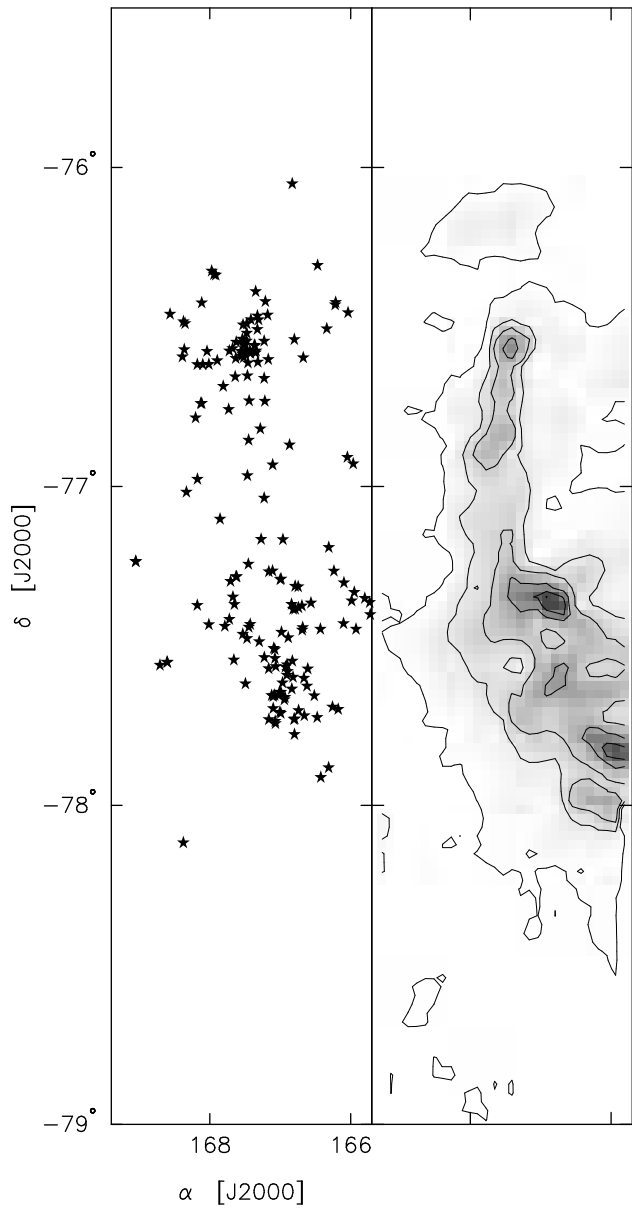


Fig. 15.— Positions of young stellar members (left panel) and extinction contours (right panel) for the Cha I star-forming region, modified from Carpenter et al. (2002) (see text)

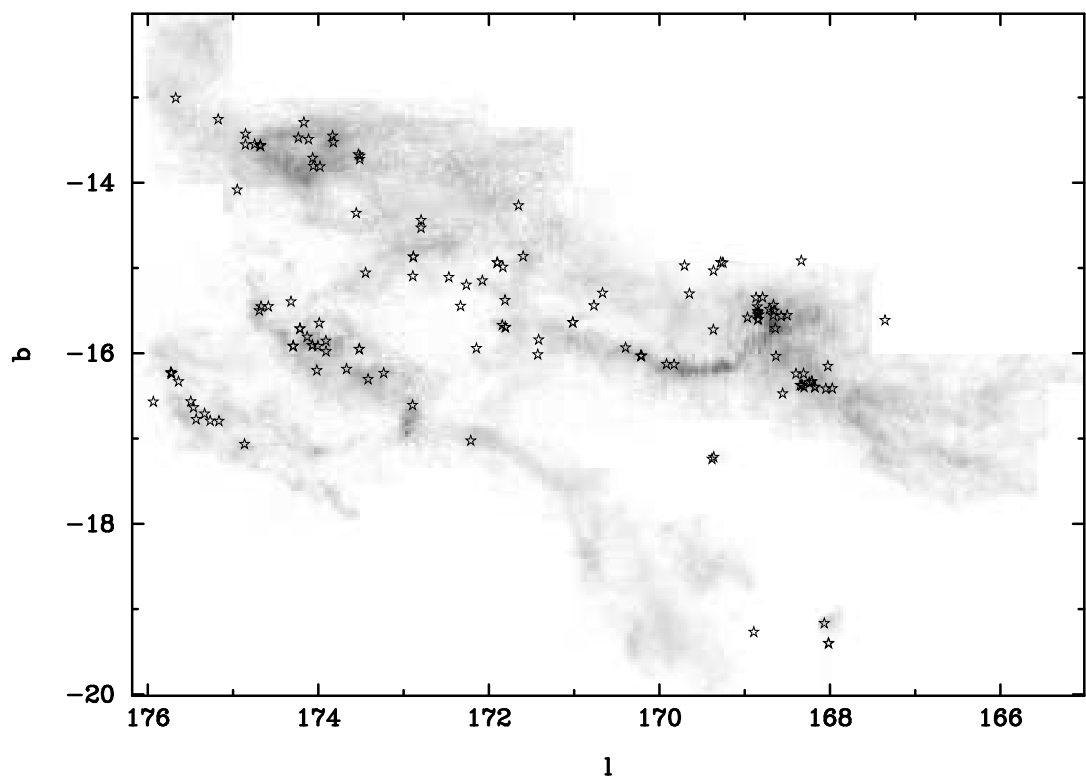


Fig. 16.— Positions of young stars and protostars superimposed upon the  $^{13}\text{CO}$  integrated emission in Taurus, the latter taken from Mizuno et al. ; (1995) (see text)